JCI The Journal of Clinical Investigation

RSV-encoded NS2 promotes epithelial cell shedding and distal airway obstruction

Rachael M. Liesman, … , Peter L. Collins, Raymond J. Pickles

J Clin Invest. 2014. https://doi.org/10.1172/JCI72948.

Research Article **Virology**

Respiratory syncytial virus (RSV) infection is the major cause of bronchiolitis in young children. The factors that contribute to the increased propensity of RSV-induced distal airway disease compared with other commonly encountered respiratory viruses remain unclear. Here, we identified the RSV-encoded nonstructural 2 (NS2) protein as a viral genetic determinant for initiating RSV-induced distal airway obstruction. Infection of human cartilaginous airway epithelium (HAE) and a hamster model of disease with recombinant respiratory viruses revealed that NS2 promotes shedding of infected epithelial cells, resulting in two consequences of virus infection. First, epithelial cell shedding accelerated the reduction of virus titers, presumably by clearing virus-infected cells from airway mucosa. Second, epithelial cells shedding into the narrow-diameter bronchiolar airway lumens resulted in rapid accumulation of detached, pleomorphic epithelial cells, leading to acute distal airway obstruction. Together, these data indicate that RSV infection of the airway epithelium, via the action of NS2, promotes epithelial cell shedding, which not only accelerates viral clearance but also contributes to acute obstruction of the distal airways. Our results identify RSV NS2 as a contributing factor for the enhanced propensity of RSV to cause severe airway disease in young children and suggest NS2 as a potential therapeutic target for reducing the severity of distal airway disease.

RSV-encoded NS2 promotes epithelial cell shedding and distal airway obstruction

Rachael M. Liesman,[1,2] Ursula J. Buchholz,[3] Cindy L. Luongo,[3] Lijuan Yang,[3] Alan D. Proia,[4] John P. DeVincenzo,[5] Peter L. Collins,[3] and Raymond J. Pickles[1,2]

[1]Department of Microbiology and Immunology and [2]Cystic Fibrosis and Pulmonary Research and Treatment Center, University of North Carolina at Chapel Hill, Chapel Hill, North Carolina, USA. [3]Laboratory of Infectious Diseases, RNA Viruses Section, National Institute of Allergy and Infectious Diseases, NIH, Bethesda, Maryland, USA. [4]Department of Pathology, Duke University Medical Center, Durham, North Carolina, USA. [5]University of Tennessee, LeBonheur Children's Medical Center and Children's Foundation Research Center, Memphis, Tennessee, USA.

Respiratory syncytial virus (RSV) infection is the major cause of bronchiolitis in young children. The factors that contribute to the increased propensity of RSV-induced distal airway disease compared with other commonly encountered respiratory viruses remain unclear. Here, we identified the RSV-encoded nonstructural 2 (NS2) protein as a viral genetic determinant for initiating RSV-induced distal airway obstruction. Infection of human cartilaginous airway epithelium (HAE) and a hamster model of disease with recombinant respiratory viruses revealed that NS2 promotes shedding of infected epithelial cells, resulting in two consequences of virus infection. First, epithelial cell shedding accelerated the reduction of virus titers, presumably by clearing virus-infected cells from airway mucosa. Second, epithelial cells shedding into the narrow-diameter bronchiolar airway lumens resulted in rapid accumulation of detached, pleomorphic epithelial cells, leading to acute distal airway obstruction. Together, these data indicate that RSV infection of the airway epithelium, via the action of NS2, promotes epithelial cell shedding, which not only accelerates viral clearance but also contributes to acute obstruction of the distal airways. Our results identify RSV NS2 as a contributing factor for the enhanced propensity of RSV to cause severe airway disease in young children and suggest NS2 as a potential therapeutic target for reducing the severity of distal airway disease.

Introduction

Human respiratory syncytial virus (RSV) is a nonsegmented, negative-sense, single-stranded RNA virus belonging to the family *Paramyxoviridae*, subfamily *Pneumovirinae*. RSV is the most common virus responsible for acute and severe lower airway disease in infants and young children, with nearly all children experiencing at least one RSV infection by the age of 2 years (1). While most RSV infections present with mild to moderate self-limiting pulmonary symptoms, in approximately 2% of cases, especially in infants who are very young (<3 months), premature, or who have underlying immunodeficiency or cardiopulmonary disease, lower airway disease is severe enough to require hospitalization (2). Worldwide, an estimated 34 million new pediatric cases of RSV-associated lower airway disease occur annually, accounting for approximately 200,000 deaths, almost all of which occur in developing countries with reduced access to standardized care (3).

Despite significant impact of RSV infection on infant morbidity and mortality, treatment options remain limited largely to supportive care. Ribavirin is the only antiviral drug currently approved for treating RSV infections, but issues of efficacy, delivery, and toxicity restrict its use to immunocompromised patients (4). Bronchodilators and anti-inflammatory steroids are widely prescribed to dampen the inflammatory consequences of RSV infection, despite evidence that these treatments provide little to no clinical benefit (5–7). Prophylactic use of passively administered neutralizing antibodies is effective in reducing RSV-associated hospitalization in susceptible populations, but these antibody treatments are expensive and inconvenient, and are limited to at-risk infants (8, 9). Licensed RSV vaccines are currently unavailable but are under active development. The high incidence of RSV infection and the potential for severe distal airway disease in vulnerable young children, combined with limited availability of therapeutic options, identifies a significant global human health need.

RSV infects the mucosal epithelium lining the human respiratory tract, predominantly targeting the columnar epithelial cells of the conducting airways. The columnar airway epithelium provides critical innate defense functions important for maintaining lung sterility. Airway epithelial cells respond to inhaled pathogens by secreting antimicrobials and recruiting inflammatory cell infiltrates important for clearing infection and subsequent tissue repair. The airway epithelium also uniquely provides mechanical clearance of inhaled pathogens by facilitating unidirectional mucus transport, largely due to synchronous beating of cilia and regulated mucin secretion. Precisely how RSV infection affects innate functions of the columnar airway epithelium and how this relates to subsequent RSV-associated disease is poorly defined, largely due to the limited availability of human airway pathology specimens obtained during early RSV infection. In the limited postmortem studies available from RSV-infected infants, it was noted that epithelial cells positive for RSV antigen were sloughed into the lumens of infected airways, leading to speculation that intralumenal accumulations of infected and necrotic epithelial cells could contribute to airway obstruction and inflammation, exacerbating airway disease (10–12). Whether sloughing of airway epithelial cells was a direct consequence of RSV-induced epithelial cell cytopathology or a bystander effect

Conflict of interest: The authors have declared that no conflict of interest exists.

Note regarding evaluation of this manuscript: Manuscripts authored by scientists associated with Duke University, The University of North Carolina at Chapel Hill, Duke-NUS, and the Sanford-Burnham Medical Research Institute are handled not by members of the editorial board but rather by the science editors, who consult with selected external editors and reviewers.

Citation for this article: *J Clin Invest.* 2014;124(5):2219–2233. doi:10.1172/JCI72948.

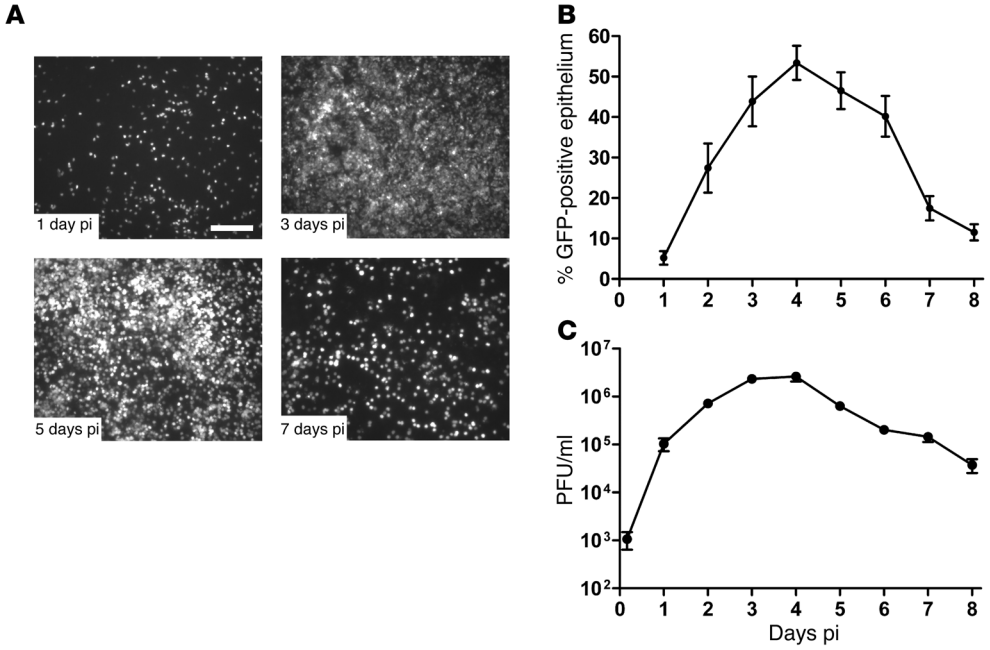

Figure 1
RSV-GFP infection, replication, and clearance in HAE cultures. (**A**) Representative en face fluorescent images of GFP-positive cells in HAE infected with RSV expressing GFP at days 1, 3, 5, and 7 pi. Scale bar: 200 μm. (**B**) The number of RSV-infected cells in HAE over time, quantified as the percentage of the epithelium surface area positive for GFP fluorescence. (**C**) Virus titers present in the airway surface fluid over time. Data (mean ± SEM) are representative of independent experiments utilizing at least 4 cultures per donor obtained from 3 different donors.

of the robust infiltration of inflammatory cells into the infected airways has been difficult to decipher in the complex in vivo environment of the lung.

We previously described an in vitro model of RSV infection of human cartilaginous airway epithelium (HAE) that recapitulates the cellular distribution and physiology of the human differentiated airway epithelium. Using this model, we and others have shown that RSV infects and spreads in HAE by preferentially infecting ciliated epithelial cells while sparing mucin-containing Goblet cells and the underlying basal epithelial cells (13, 14). These in vitro findings are supported by histologic studies of cartilaginous airways from RSV-infected patients that also demonstrate the preferential tropism of RSV for ciliated cells (10). Tropism for ciliated cells is not unique to RSV, as other RNA viruses, including paramyxoviruses, coronaviruses, and avian influenza viruses, have been shown to preferentially infect ciliated cells in the HAE model (15–17).

Our previous studies demonstrated that RSV infection of human ciliated cells in HAE was minimally cytopathic, at least within the first 48 hours of infection (14). The lack of direct RSV-induced cytopathology was in contrast to the rapid and robust cytopathology documented in HAE infected by influenza viruses (18). In the present study, we have expanded our earlier studies with RSV to track the fate of RSV-infected ciliated cells over time and to determine consequences of infection potentially important for pathogenesis. By tracking the fate of ciliated cells infected by RSV in vitro, we identified a unique consequence of RSV infection whereby infected ciliated cells rapidly transitioned from a columnar to a rounded cell morphology and were then extruded from the otherwise intact epithelium. Once shed, the detached RSV-infected cells were incorporated into lumenal mucus secretions of HAE and were transported by the directional flow of mucus secretions. Using RSV gene deletion mutants, ciliated cell rounding after RSV infection was attributed to the RSV non-structural 2 (NS2) protein. Gain-of-function experiments using recombinant, GFP-expressing parainfluenza virus 3 (PIV3-GFP) engineered to express RSV NS2 (PIV3-NS2) demonstrated that ciliated cells infected with PIV3-NS2, but not with PIV3, became rounded and morphologically indistinguishable from ciliated cells infected with RSV. To explore potential in vivo functions of RSV NS2 expression, we infected the airways of Golden Syrian hamsters with PIV3-NS2 or PIV3 and show that PIV3-NS2 caused rapid shedding of infected epithelial cells from the airway epithelium, which coincided with accelerated clearance of virus infection from hamster lungs. These studies also revealed an unexpected consequence of PIV3-NS2 infection of the narrower-diameter bronchiolar airways, in which PIV3-NS2 but not PIV3 caused sufficient intralumenal accumulations of shed epithelial cells to partially or fully occlude the bronchiolar airway lumens. These findings suggest that acute, distal airway obstruction, a common feature of RSV infection in infants, may be due to the rapid shedding of RSV-infected bronchiolar epithelial cells into the airway lumen and that this event is a direct consequence of RSV NS2 expression. To our knowledge, these studies provide the first description of the unique fate of RSV-infected columnar airway epithelial cells and identify a novel property of the RSV NS2 protein as promoting this event.

Results

Kinetics of RSV replication in HAE. The kinetics of RSV infection in HAE was measured by inoculating the apical surface of cultures with a recombinant RSV expressing GFP inserted between the phosphoprotein (P) and matrix (M) genes (3×10^5 PFU; MOI ~1), and the numbers of GFP-positive cells and titers of released virus were determined every 24 hours for 8 days. Representative en face images of GFP-positive cells and quantification of the percentage of epithelium surface area positive for GFP across HAE obtained from multiple tissue donors are shown in Figure 1, A and B, respectively. At day 1 post-inoculation (pi), RSV infection resulted in 5% of the epithelium surface area positive for GFP, and over time the extent of infection steadily increased as virus infection spread, with 53% of the epithelium surface area being GFP-positive

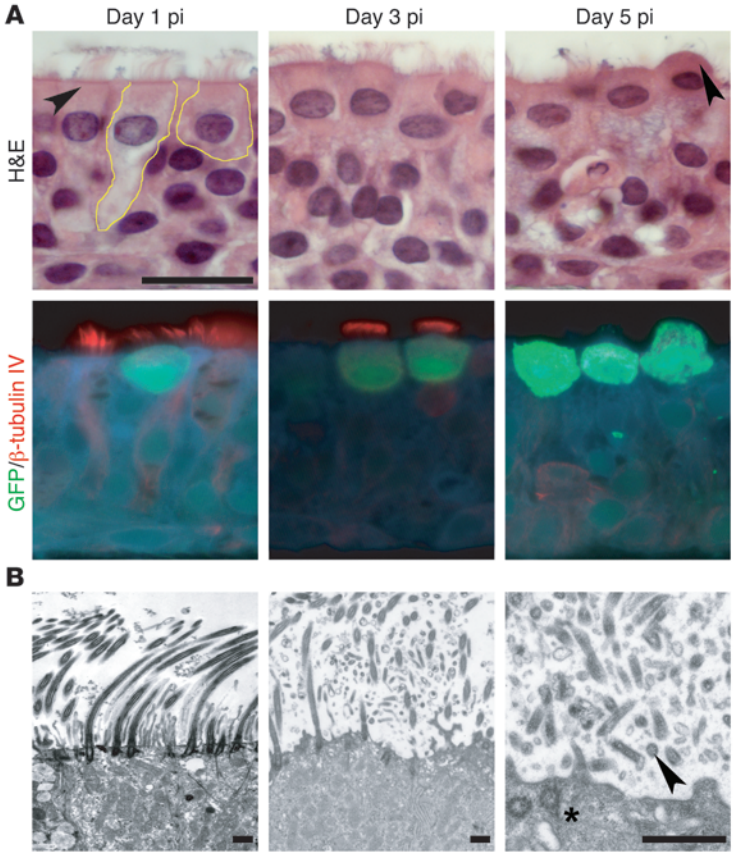

Figure 2
Morphologic and structural changes in RSV-infected ciliated columnar cells. (**A**) Representative histologic sections of HAE inoculated with RSV expressing GFP and counterstained with H&E or immunoprobed for GFP (green) and β-tubulin IV (red) at days 1, 3, and 5 pi. Yellow outlines at top left depict the different ciliated cell morphologies seen in RSV-infected HAE, where noninfected ciliated cells are columnar and RSV-infected ciliated cells exhibit rounded morphology. Arrowheads indicate robust apical terminal web in noninfected ciliated cells (top left), which thins in RSV-infected ciliated cells with rounded morphology (top right). Images are representative of independent experiments with 4 different donor cultures. Scale bar: 10 μm. (**B**) Representative TEM of cross-sections of the apical surfaces of noninfected (left) and RSV-GFP–infected (center, right) HAE. Arrowhead indicates particulates showing virus-like morphology. Asterisk indicates disorganized basal bodies. Scale bars: 1 μm.

by day 4 pi. Beyond day 4 pi, the numbers of GFP-positive cells declined rapidly, and by day 8 pi, infected cell numbers approximated those at day 1 pi In agreement with previous studies (14), only ciliated cells expressed GFP, which confirmed RSV tropism for ciliated cells in this model. On average, ciliated cells represented approximately 90% of the surface columnar epithelial cells in HAE, indicating that approximately 60% of available ciliated cells were infected by RSV at the time of maximal infection (day 4). Throughout infection, HAE cultures remained intact based on gross visual inspection, as previously described (14, 17).

RSV titers in washes harvested from the apical surfaces of HAE paralleled the numbers of GFP-positive cells (Figure 1C). RSV titers steadily increased proportionate to the numbers of GFP-positive cells during the first 3 days of infection, reaching maximal titers by day 4 pi (2.6×10^6 PFU/ml). Once maximal, virus titers declined proportionate to the loss of GFP-positive cells, and by day 8 pi, virus titers had fallen by 2 logs compared to those at day 4 pi (Figure 1C). The rapid net loss of RSV infection from HAE between days 4 and 8 pi suggests that most of the RSV-infected ciliated cells were cleared from the epithelium during this period and, as HAE are pure populations of epithelial cells, that clearance of infected ciliated cells occurred in the absence of immune cell–mediated clearance mechanisms.

A distinctive morphologic change in RSV-infected columnar airway cells. To investigate how RSV-infected (GFP-positive) ciliated cells were cleared from HAE, we used histologic analysis to track the fate of infected ciliated cells over time. These studies revealed that RSV-infected ciliated cells underwent a distinctive morphologic transition from the native columnar cell morphology to a rounded cell morphology while remaining embedded in the epithelium (Figure 2A). Ciliated epithelial cells of both human cartilaginous airway epithelium in vivo and HAE cultures in vitro are characteristically columnar, with individual ciliated cells spanning the depth of the epithelium and the ciliated cell tail intercalating into the underlying basal epithelial cell layers. Histologic assessment of ciliated cell rounding in vitro revealed that RSV infection caused a rapid retraction of the ciliated cell tails, which resulted in the infected cell assuming a rounded shape. Only GFP-positive ciliated cells (i.e., infected with RSV) exhibited rounded cell morphology, and no GFP-positive cells were observed that retained the native columnar shape of ciliated cells, suggesting that ciliated cell rounding was a direct consequence of RSV infection.

Ciliated cells infected by RSV also began to bulge from the epithelial layer into the lumenal compartment and were eventually extruded from the epithelium (Figure 2A). During the extrusion process, the bulging apical membranes of RSV-infected cells progressively lost apical structural components of ciliated cells, including cilia, as demonstrated by loss of β-tubulin IV immunoreactivity (Figure 2A) and a marked thinning of the cytoskeletal terminal web (see arrows in Figure 2A). Despite significant disruption of apical structures in these bulging ciliated cells, the cells retained GFP fluorescence, suggesting that plasma membrane permeability was not overtly compromised (Figure 2A). High-power transmission electron microscopy (TEM) studies of noninfected and RSV-infected HAE, fixed to preserve the hydrated external environment of the HAE lumenal surface, confirmed that RSV infection resulted in the disintegration of apical structures, most notably cilia shafts and microvilli (Figure 2B). Basal bodies, usually organized directly below emerging cilia shafts, were often disorganized in the cytoplasm of RSV-infected ciliated cells (asterisk in Figure 2B). Clouds of particulate matter in the external lumenal environment were composed of fragmented cilia and microvilli directly above bulging RSV-infected ciliated cells. It is reasonable to presume that these particulate clouds also contain progeny RSV virions and, on occasion, structures resembling RSV virions were detected (arrow in Figure 2B). More conclusive identification of RSV virions in these clouds was technically challenging, as immunogold labeling of virus proteins would not discriminate between infectious progeny virions and virus proteins associated with fragmented cellular debris.

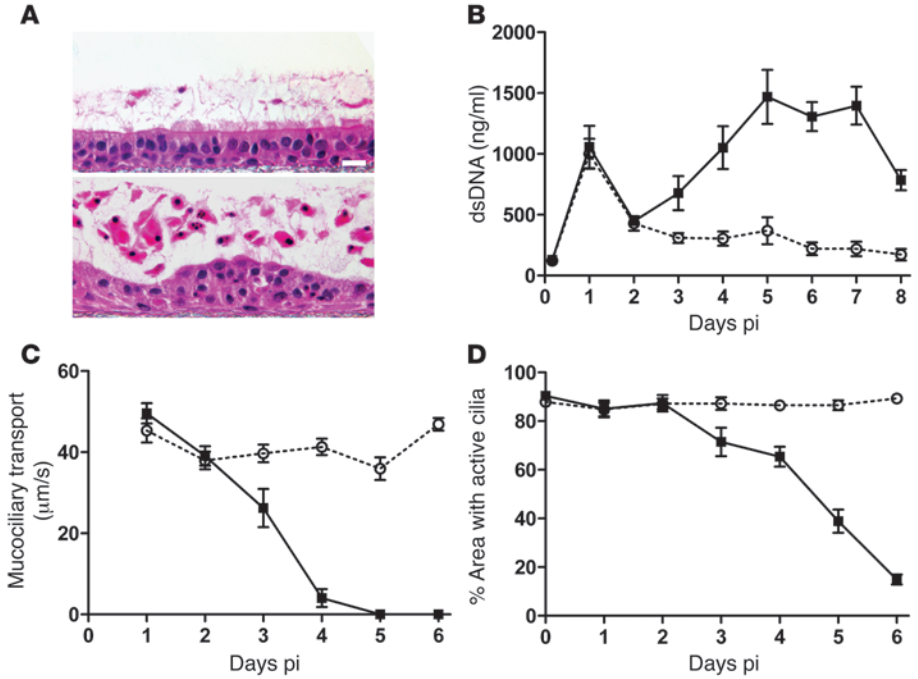

Figure 3

Ciliated cell shedding and loss of cilia activity during RSV-GFP infection of HAE. (**A**) Representative images of histological cross-sections of noninfected HAE (top) or HAE infected with RSV expressing GFP (bottom) fixed at day 5 pi using a fixation protocol to preserve the content and depth of airway surface secretions. Scale bar: 20 μm. (**B**) Concentration of dsDNA as an index for numbers of shed cells present in apical washes harvested every 24 hours from noninfected (white circles) or RSV-infected (black squares) HAE. Data (mean ± SEM) were derived from 4 cultures per donor for 4 different donors. (**C**) Fluorescent bead velocity as an index of mucus transport rates on the apical surfaces of noninfected (white circles) or RSV-infected (black squares) HAE at indicated times pi. Data (mean ± SEM) represent 3–6 cultures per donor for 3 different donors. (**D**) Surface area of active cilia beat on noninfected (white circles) or RSV-infected (black squares) HAE. Data (mean ± SEM) represent 4 cultures. Data in **B**–**D** show significant differences at day 3 pi ($P < 0.05$) and at all time points thereafter ($P < 0.001$), as determined by unpaired *t* test.

Shedding of epithelial cells from RSV-infected HAE. To further assess the cytopathology of RSV-infected cells, we examined histologic sections of noninfected and RSV-infected HAE fixed to preserve airway surface secretions accumulated over a 5-day period. In noninfected HAE, only occasional detached epithelial cells were present in accumulated mucus secretions (Figure 3A, top). In contrast, RSV-infected cultures contained large numbers of detached epithelial cells embedded in an increased mucus layer (Figure 3A, bottom). In addition to the increased number of detached cells in mucus secretions, the underlying intact epithelium of RSV-infected cultures was irregular in appearance, largely due to the rounded morphology of infected ciliated cells remaining in the epithelium. An overall decrease in cilia abundance also was noted in the RSV-infected epithelium.

We quantified the extent and kinetics of epithelial cell shedding from RSV-infected HAE cultures by determining the amount of dsDNA present in daily washes of the lumenal surfaces of noninfected and RSV-infected HAE (Figure 3B). Apical washes consistently contained increased amounts of dsDNA at day 1 pi for both noninfected (mock-inoculated) and RSV-infected HAE, which we attribute to consequences of the inoculation procedure. However, by day 3 pi, there was a clear difference between RSV-infected and noninfected HAE in the amount of dsDNA present in apical washes, as dsDNA consistently increased in RSV-infected HAE cultures, reaching maximal levels at days 5 to 7 pi Amounts of dsDNA in apical washes from noninfected HAE remained low and constant over the same time period. The increased dsDNA in apical washes closely correlated with the loss of GFP-positive epithelial cells from HAE (Figure 1B), indicating the usefulness of dsDNA as a marker for the numbers of shed epithelial cells in airway secretions in vitro.

Overall, these observations suggest that the loss of GFP-positive cells from RSV-infected HAE is predominately due to shedding of the infected ciliated cells from the airway mucosa. RSV-infected epithelial cells, while rounded and extruding from the epithelium, exhibited no obvious nuclear abnormalities (Figure 3A) and were negative for TUNEL staining (data not shown), indicating that infected cells during the shedding process remained viable. Infected cells also retained GFP fluorescence, suggesting that the plasma membrane of infected cells remained intact. In contrast, shed and detached epithelial cells in mucus secretions on the apical surface of HAE displayed well-characterized nuclear structural changes indicative of cell death, and pyknosis (nuclear shrinkage), karyorrhexis (nuclear fragmentation), and karyolysis (nuclear dissolution) were noted in shed epithelial cells (Figure 3A). These findings demonstrate that RSV-infected ciliated cells do not undergo overt cell death while embedded in the epithelium and that cell death in situ does not play a significant role in the clearance of RSV-infected cells from HAE. Rather, infected cells undergo cell death after becoming completely detached from the epithelium, although we have not been able to determine the precise kinetics of when shed cells die. We have also been unable to identify cellular mechanisms leading to death of shed cells. Nevertheless, since the reduction of RSV titers in HAE paralleled the loss of GFP-positive cells, we propose that shedding of RSV-infected ciliated cells, and not death while cells are embedded in the epithelium, represents the primary mechanism for clearing RSV infection from a differentiated airway epithelium, at least in vitro.

Effects of RSV infection on mucociliary transport. Extensive shedding of cells onto the lumenal surface of RSV-infected HAE suggests that, in vivo, this cellular material may be cleared from the airway lumen by mechanical clearance mechanisms, such as mucociliary transport (MCT). In vitro, we often observed shed and detached GFP-positive cells being transported within mucus secretions across the surface of cultures. Since directional transport of mucus secretions in HAE is dependent on coordinated cilia beat, the potential impact of RSV infection on the effectiveness of cilia function may adversely affect the ability of the airways to mechanically clear infection. We tested the consequence of RSV infection on

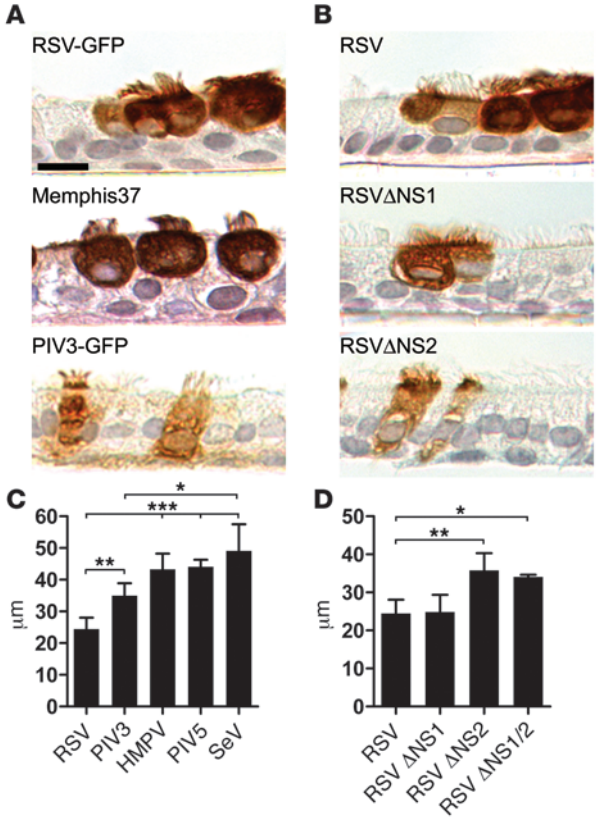

Figure 4
RSV-induced ciliated cell rounding is unique to RSV infection and is due to expression of the RSV NS2 protein. (**A**) Representative images of histologic cross-sections of fixed and paraffin-embedded HAE infected with recombinant RSV-GFP, low-passage clinical isolate RSV Memphis 37, or recombinant PIV3-GFP. Infected cells were detected at day 3 pi using an anti-RSV antibody or anti-PIV3 antibody, as appropriate. Scale bar: 10 μm. (**B**) Representative images of histologic cross-sections of HAE infected with RSV, or gene deletion mutants RSVΔNS1 and RSVΔNS2. All viruses express GFP. (**C** and **D**) Height of infected ciliated cells (mean ± SD) was determined using confocal microscopy of fixed but unprocessed HAE infected with RSV, PIV3, HMPV, PIV5, or SeV or the RSV gene deletion mutants RSVΔNS1, RSVΔNS2, and RSVΔNS1/2. All viruses expressed GFP. At least 100 infected cells in cultures obtained from 3 different donors were measured. $^{*}P < 0.05$, $^{**}P < 0.01$, $^{***}P < 0.001$, 1-way ANOVA with Tukey's post-hoc test.

directional transport of particulates present in airway secretions by measuring MCT rates of 1-μm fluorescent beads transported across the lumenal surface of HAE (Figure 3C). For noninfected HAE, MCT rates of approximately 40 μm/s were maintained for 6 consecutive days of experimental analysis. For RSV-infected HAE, MCT rates approximated those of noninfected HAE during the first 2 days of RSV infection, despite infection of approximately 20% of the epithelium surface. However, by day 3 pi, RSV-infected HAE demonstrated a significant decline in MCT rate, and by day 4 pi, when approximately 60% of the epithelium surface was infected, MCT rates had fallen drastically to below 5 μm/s. By day 5 pi, bead transport in RSV-infected HAE had ceased.

To determine whether loss of MCT after RSV infection was directly associated with loss of cilia function, we also quantified the percentage of the epithelium surface that displayed beating cilia at each time point (Figure 3D). In noninfected HAE, approximately 90% of the epithelium surface possessed active cilia, and this level was maintained over 6 consecutive days of analysis. A similar extent of cilia activity was measured during the first 2 days of RSV infection, indicating that cilia activity of infected cells was not significantly affected early during infection, similar to our previous findings (14). However, beginning at day 3 pi, the area of active cilia progressively declined, resulting in only 38% of the epithelium surface displaying active cilia by day 5 pi and 10% by day 6 pi. These results suggest that RSV infection has little effect on the ability of the ciliated epithelium to generate MCT within the first few days of infection. However, as the numbers of infected cells increased and as infection of individual cells resulted in apical membrane cytopathology, RSV infection can abolish MCT. We noted that at day 3 pi and day 4 pi, although the area of cilia activity was high, MCT rates had rapidly declined. Such declines in MCT rate prior to significant losses in the area of active cilia may be explained by subtle but deleterious effects of RSV infection on coordinated cilia beat, such as cilia beat asynchrony and subsequent disruption of unidirectional transport. Indeed, high-speed video images of RSV-infected ciliated cells reveal visual evidence of cilia beat asynchrony prior to the loss of cilia structures (Supplemental Figure 1 and Supplemental Video 1; supplemental material available online with this article; doi:10.1172/JCI72948DS1). Taken together, these data suggest that, at least until day 3 pi, RSV-infected HAE cultures maintain sufficient MCT to transport infected cells shed across the airway surface, and that cell shedding may represent a previously unidentified mechanism to enhance MCT-mediated clearance of RSV infection from the airways.

Cell rounding is unique to RSV among a number of common paramyxoviruses. We also investigated whether RSV-induced rounding of ciliated cells occurred following infection with other respiratory viruses known to infect ciliated cells in HAE. Ciliated cells infected by PIV serotypes 1, 2, 3, or 5, Sendai virus (SeV), or human metapneumovirus (HMPV) failed to exhibit ciliated cell rounding (Figure 4, A and C, and data not shown). As an index of cell rounding, we measured the height of GFP-positive cells using confocal microscopy xz sections. Ciliated cells infected by RSV were significantly shorter, due to cell rounding, than those infected by the other GFP-expressing respiratory viruses that were tested (Figure 4C). Our studies utilized a recombinant RSV A2 strain expressing GFP, and we confirmed that cell rounding was not an artifact of the recombinant virus or expression of GFP, as a recombinant RSV without GFP (GP1), the biologically derived RSV from which the recombinant was generated (HEp-4), and a wild-type RSV strain of subgroup B all caused rounding of infected ciliated cells identical to the recombinant GFP-expressing virus (data not shown). Because studies have described phenotypic differences between highly passaged RSV strains and clinical isolates, we confirmed that a recently isolated, minimally passaged, clinical strain of RSV (RSV Memphis 37) caused infected ciliated cells to round with morphology indistinguishable from those cells infected by recombinant GFP-expressing RSV (Figure 4A). Overall, these data suggest that ciliated cell rounding is a unique consequence of RSV infection.

Columnar cell rounding is associated with expression of the NS2 gene. We speculated that the unique morphologic phenotype induced in ciliated cells by RSV infection might be due to the expression of specific RSV genes. We explored this possibility by infecting human ciliated cells with recombinant, GFP-expressing RSVs

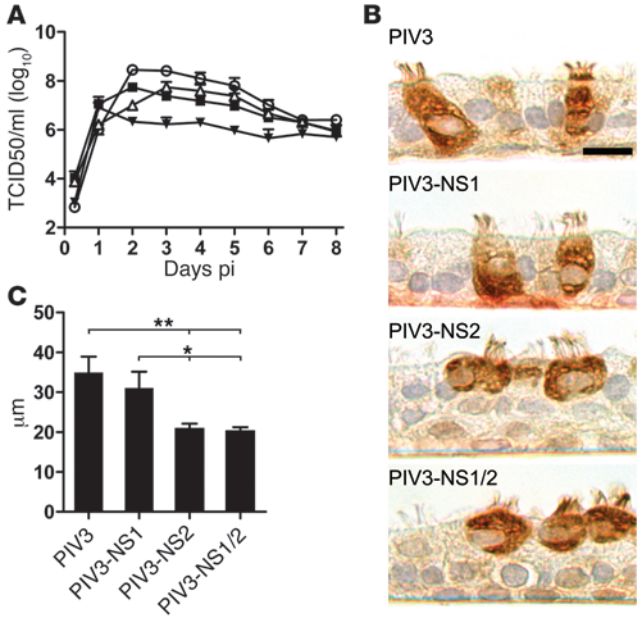

Figure 5

Expression of RSV NS2 in ciliated cells using PIV3 results in infected cell rounding. (**A**) Growth kinetics of recombinant PIV3 (white circles) and PIV3 expressing either RSV NS1 (PIV3-NS1, black squares), NS2 (PIV3-NS2, white triangles) or both NS1 and NS2 (PIV3-NS1/2, black triangles) in HAE. All viruses expressed GFP. Virus titers in apical washes were assessed at 24-hour intervals. Data (mean ± SEM) represent 4 cultures per donor with cultures from 3 different donors. (**B**) Representative images of histologic cross-sections of HAE infected with PIV3, PIV3-NS1, PIV3-NS2, or PIV3-NS1/2. Infected cells were detected with an anti-PIV3 antibody. Scale bar: 10 μm. (**C**) Height of infected cells (mean ± SD) was determined as described in Figure 4. $^{*}P < 0.05$, $^{**}P < 0.01$, 1-way ANOVA with Tukey's post-hoc test.

from which individual viral genes had been deleted. These studies revealed that infection of ciliated cells by a mutant RSV with deletion of the two NS genes, NS1 and NS2 (RSVΔNS1/2), failed to cause rounding of infected ciliated cells (Figure 4D). Instead, ciliated cells infected with this mutant retained the native columnar morphology and resembled the morphology of ciliated cells infected by other respiratory viruses, such as PIV3. Evaluation of RSV mutants deleted of NS1 or NS2 genes (RSVΔNS1 and RSVΔNS2) showed that RSVΔNS1 induced ciliated cell rounding indistinguishable from that of RSV expressing a full complement of RSV genes, suggesting that NS1 was not responsible for the cell-rounding phenotype (Figure 4, B and D). In contrast, ciliated cells infected by RSVΔNS2 did not round and maintained columnar morphology identical to that following RSVΔNS1/2 infection (Figure 4, B and D). These differential effects of the NS-deleted viruses were not due to significant differences in mutant virus replication, as both RSVΔNS1 and RSVΔNS2 were similarly attenuated for replication compared with RSV in cell lines (19) and HAE (Supplemental Figure 2A). Overall, these experiments indicate that expression of NS2, in the context of RSV infection, is necessary for RSV-induced ciliated cell rounding.

Expression of NS2 by recombinant PIV3 mimics RSV-induced cell morphology. Since PIV3, like RSV, exclusively infects ciliated cells in HAE cultures but does not cause rounding of ciliated cells, we used recombinant PIV3 to deliver RSV NS1, NS2, or both genes to ciliated cells in the absence of other RSV genes. Recombinant PIV3 was engineered to express GFP and NS2 (PIV3-NS2), NS1 (PIV3-NS1), or both NS1 and NS2 (PIV3-NS1/2), and the consequences of infection compared with PIV3 expressing GFP alone were assessed. In each case, GFP was inserted between the P and M genes, and the RSV gene(s) were inserted between the HN and L genes. All recombinants were readily recovered, and infection and growth were assessed in non-polarized epithelial cell lines and HAE cultures. In non-polarized epithelial cell lines, recombinant PIV3 viruses expressing RSV NS genes and GFP were slightly attenuated for growth compared with PIV3 expressing GFP alone (Supplemental Figure 2, B and C). Similar to cell lines, in HAE, all 3 PIV3 viruses expressing RSV NS genes exhibited modest growth attenuation compared with PIV3, despite similar levels of infection at day 1 pi (Figure 5A). Growth of PIV3-NS2 and PIV3-NS1 was equally attenuated in HAE, replicating to titers approximately 1 log lower than PIV3 at day 3 pi, the time of peak replication. Growth of PIV3-NS1/2 was more severely attenuated, producing titers 2 logs lower than PIV3 at the time of peak replication. This observed attenuation presumably reflected the increased genome length and gene number of the PIV3 viruses with inserted RSV NS genes, although the possibility exists that the RSV NS proteins had direct inhibitory effects on replication.

In HAE cultures, ciliated cells infected by PIV3 or PIV3-NS1 maintained native columnar morphology, whereas ciliated cells infected by PIV3-NS2 or PIV3-NS1/2 underwent cell rounding, with significantly shortened cell heights (Figure 5, B and C) and closely resembled ciliated cell morphology after RSV infection. The observation that PIV3-NS1/2 and PIV3-NS2 caused cell rounding indistinguishable from that caused by RSV suggested that NS2 mediated this effect independent of the expression of NS1 or other RSV proteins.

NS2 expression adversely affects ciliated cell structure and function. In addition to similar overall morphology of ciliated cells infected by PIV3-NS2 and RSV, closer examination of ultrastructural features of the apical surfaces of ciliated cells infected by PIV3-NS2 or PIV3-NS1/2 recapitulated those of RSV-infected cells. Characteristics of RSV-infected ciliated cells such as bulging apical membranes, thinning of the terminal web, and loss of cilia and microvilli were evident in, and indistinguishable between, ciliated cells infected by RSV, PIV3-NS2, and PIV3-NS1/2 (Figure 6A).

Functional studies measuring the extent of cilia activity in HAE infected by the recombinant viruses demonstrated that PIV3-NS2 and PIV3-NS1/2 infection resulted in a marked decline in the surface area of epithelium displaying cilia activity within the first 4 days of infection (Figure 6B). In contrast, PIV3 infection did not affect the extent of cilia activity until day 5 pi. PIV3-NS1, despite robust infection, had little effect on cilia activity within the 6 days of experimental analysis. These data suggest that PIV3 infection was less cytopathic to cilia activity compared with PIV3-NS2, indicating that NS2-promoted cell rounding may also be associated with disruption of cilia or cilia scaffolding complexes in infected cells. We also noted that NS1 may further reduce the moderate cytopathology evident after PIV3 infection. These findings are intriguing, as they point to divergent effects of RSV NS1 and NS2 on ciliated cell cytopathology. However, as noted above, experiments with PIV3-NS1/2 indicate these divergent effects of NS2 and NS1 expression on

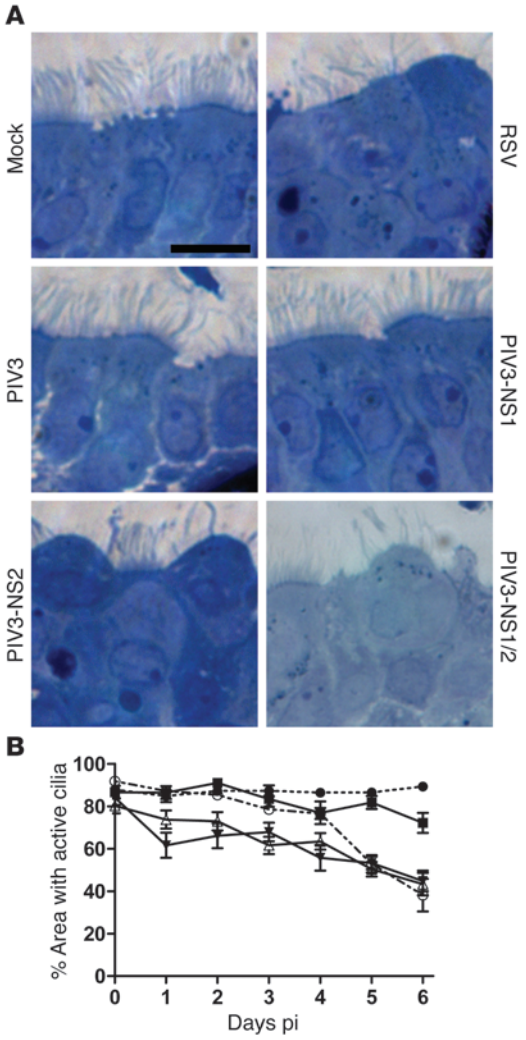

Figure 6
Expression of RSV NS2 by PIV3 in HAE cultures mimics RSV-induced cytopathology at the apical surface of ciliated cells. (**A**) Representative images of histologic sections of noninfected HAE, or HAE infected by RSV, PIV3, PIV3-NS1, PIV3-NS2, or PIV3-NS1/2 fixed at day 2 pi showing similar apical membrane disruption in ciliated cells infected by RSV, PIV3-NS2, and PIV3-NS1/2. Richardson's counterstain was used. Scale bar: 10 μm. (**B**) Surface area of active cilia beat on noninfected HAE (black circles, dotted line) or HAE infected with PIV3 (white circles), PIV3-NS1 (black squares), PIV3-NS2 (white triangles), or PIV3-NS1/2 (black triangles). Data (mean ± SEM) represent quadruplicate cultures. All viruses expressed GFP.

ciliated cell cytopathology are dominated by the effects of NS2 when both NS proteins are expressed together, as occurs with PIV3-NS1/2 or RSV infection.

Effects of RSV NS2 on PIV infection of airway epithelium in vivo. We next used the PIV3 viruses expressing RSV NS genes to test the morphologic consequences of RSV NS2 expression in vivo. Because PIV3 poorly infects the airway epithelium of mice, we chose Golden Syrian hamsters as our in vivo model, as they are a well-documented useful model of PIV3 airway infection (20). We first focused on the hamster nasal respiratory airway epithelium, as this pseudostratified columnar epithelium contains ciliated and mucin-containing (goblet) cells at densities similar to those of columnar cells in HAE cultures and human cartilaginous airway epithelium in vivo. Hamsters were inoculated intranasally with PIV3, PIV3-NS2, or PIV3-NS1 (10^6 PFU). Maximal virus titers were reached in the nasal tissue by day 3 pi, and we observed equal but modest attenuation of growth of PIV3-NS1 and PIV3-NS2 compared with PIV3 (Figure 7A), similar to attenuation in HAE (Figure 5A).

Identification of virus-infected epithelial cells by immunodetection of PIV3 antigen in histologic sections of hamster nasal epithelium at day 3 pi showed that all recombinant PIV3 viruses infected ciliated columnar cells but not mucin-containing Goblet columnar cells of the hamster nasal respiratory epithelium (Figure 7B). While ciliated cells infected by PIV3 or PIV3-NS1 retained the native columnar cell morphology, cells infected by PIV3-NS2 exhibited rounded cell morphology and resembled human ciliated cells infected by PIV3-NS2 or RSV in vitro. Morphometric analysis of infected ciliated cell height in histologic sections of hamster nasal respiratory epithelium revealed a significant shortening of ciliated cells infected by PIV3-NS2 compared with those infected by PIV3 or PIV3-NS1 (Figure 7C), reproducing the phenotype seen in HAE (Figure 5B). In PIV3-NS2–infected hamster nasal cavities, virus antigen–positive cells were occasionally observed while shedding from the epithelium into the airway lumen, but unlike what was observed in HAE, accumulations of shed, virus-infected epithelial cells after PIV3-NS2 infection were rarely noted in the nasal cavity, suggesting that epithelial cells shed from the epithelium were rapidly cleared from the airway lumen, presumably by mechanical clearance mechanisms.

Next we compared the consequences of PIV3 and PIV3-NS2 infection in the lungs of hamsters. Because PIV3-NS1 infection did not induce ciliated cell rounding in HAE or hamster nasal epithelium, we focused our lower airway studies on the comparison of PIV3 versus PIV3-NS2 infection. In hamsters inoculated with PIV3, histologic analysis of whole lungs after day 3 pi showed viral antigen distributed throughout the conducting airway epithelium of the large bronchial and small bronchiolar airway regions (Figure 8, A and B, respectively). Although virus antigen was occasionally detected in cells of the alveolar regions, the majority of infected cells were restricted to the conducting airways. PIV3-infected epithelial cells of both large and small airways retained columnar morphology and remained embedded in the epithelium, similar to PIV3-infected epithelial cells in HAE cultures.

In contrast, in hamsters infected by PIV3-NS2 for 3 days, all virus antigen–positive cells in the larger-diameter airways were rounded and either shedding from or fully detached from the underlying intact epithelium (Figure 8A). The smaller-diameter bronchiolar airways similarly showed extensive rounding and detachment of epithelial cells infected by PIV3-NS2 (Figure 8B). Remarkably, the bronchiolar airway lumens contained accumulations of shed, virus antigen–positive cells (Figure 8B), the extent of which was sufficient to cause partial to complete occlusion of the bronchiolar airway lumens (Figure 8C). Although shed cell accumulation in bronchioles was dramatic at day 3 pi, it was also transient, and by day 5 pi almost all evidence of bronchiolar airway occlusion and infection was absent, suggesting that the cell accumulations were effectively cleared from the airway lumens (Figure 8B). The rapid clearance of virus-infected cells from within the bronchiolar airway lumen was also noted in the bronchial airways at day 5 pi (Figure 8A). In contrast to the consequences of PIV3-NS2

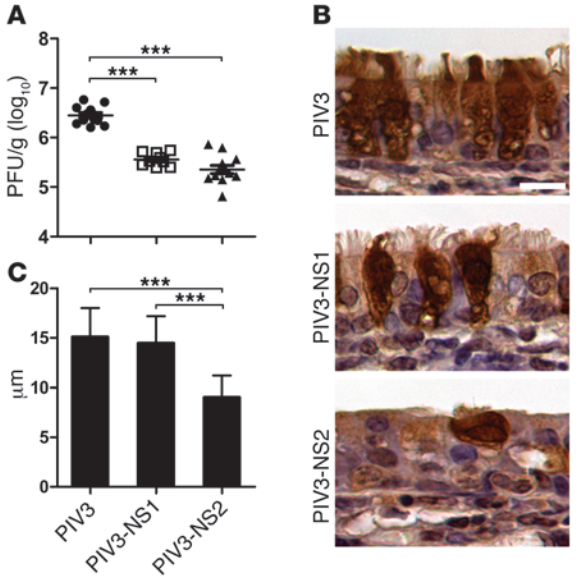

Figure 7
PIV3-NS2 causes ciliated cell rounding in the hamster nasal respiratory epithelium in vivo. (**A**) The nasal epithelium of Golden Syrian hamsters was inoculated with 10^6 PFU of PIV3 (black circles), PIV3-NS1 (white squares), or PIV3-NS2 (black triangles), and virus titers in the nasal turbinates were determined at day 3 pi. Data (mean ± SEM) represent 3 independent experiments with a total of 9 to 12 animals. (**B**) Representative images of histologic cross-sections of hamster nasal respiratory epithelium infected with PIV3 (top), PIV3-NS1 (center), or PIV3-NS2 (bottom). Virus antigen was detected at day 3 pi with an anti-PIV3 antibody. Scale bar: 10 μm. (**C**) Height of infected ciliated cells (mean ± SD) was determined by measuring height of virus antigen–positive cells from fixed tissue sections, with at least 200 cells analyzed across 3 individual animals. All viruses expressed GFP. ***$P < 0.001$, 1-way ANOVA with Tukey's post-hoc test.

infection, the robust PIV3 infection of the bronchial and bronchiolar airway epithelium at day 3 pi remained largely unaltered by day 5 pi, indicating that PIV3-infected cells were not cleared from the epithelium as effectively as those infected by PIV3-NS2 (Figure 8, A and B).

To determine whether the more effective clearance of virus-infected cells following PIV3-NS2 infection influenced viral load in the lung, we harvested hamster lung tissues inoculated with PIV3-NS2 or PIV3 at days 1, 2, 3, 5, and 7 pi and measured whole lung virus titers. These data revealed a strong temporal correlation between the extent of virus antigen–positive cells and lung viral titers. Specifically, although PIV3 and PIV3-NS2 titers were similar at days 1 and 2 pi, PIV3 titers declined by less than 1 log between days 3 and 5 pi, whereas during the same time period PIV3-NS2 titers rapidly fell by almost 3 logs (Figure 8D). Infection by both viruses was completely cleared from the lungs by day 7 pi. Throughout the experiments, hamsters showed no clinical signs of illness, as reported in previous studies of PIV3 infection of hamster airways (20). This is not surprising given the semi-permissive nature of PIV3 infection in this non-native host.

In contrast to HAE and hamster nasal epithelium studies in which PIV3 only infected ciliated cells, we noted that PIV3 and PIV3-NS2 infected both ciliated and non-ciliated columnar cells in the lower airways. We also noted that PIV3-NS2–infected cells shed into the small airways exhibited an unusual pleomorphic morphology compared with cells shed from HAE or the hamster nasal respiratory epithelium. Shed PIV3-NS2–infected lower airway cells were swollen and at times bi-nucleated, with cell bodies protruding from the intact epithelium into the airway lumen (Figure 9A). Using cytokeratin 18 as an immunomarker for epithelial cells, we confirmed that the infected, shedding, and accumulated cells were epithelial cells, as expected (Figure 9A).

To ascertain whether the morphologic consequences of PIV3-NS2 infection of hamster lower airways resembled those in lower airways of humans infected by RSV, we probed histologic sections of autopsy lung tissues obtained from RSV-infected patients for viral antigen. Assessment of pseudostratified columnar airway epithelium, indicative of larger airway regions, showed clear evidence of RSV antigen–positive epithelial cells embedded in the epithelium, displaying shortened, rounded cell morphology (Supplemental Figure 3B). Occasionally, RSV antigen–positive cells were also detected detached in the airway lumen, suggestive of shed, virus-infected cells that had not fully cleared from the airway. Examination of the distal bronchiolar airways revealed bronchiolar lumens partially or fully occluded by pleomorphic epithelial cells positive for RSV antigen and in some cases in the process of shedding into the airway lumen (Figure 9B, Supplemental Figure 3A). Swollen and bi-nucleated cells were also observed in the airway lumen of these regions. These observations indicated that the morphologic changes, cell shedding, and small airway occlusions observed in hamster distal airways infected by PIV3-NS2 resembled the consequences of RSV infection of human lower airways detected in postmortem samples.

Discussion

RSV is the most important viral agent of lower airway disease in infants and young children and is commonly associated with severe bronchiolitis in these populations. In infants, bronchiolitis caused by RSV is documented to be more severe and prolonged than bronchiolitis caused by other etiologies, including PIVs or rhinoviruses (21, 22). A recent study of young children with acute respiratory illness found that those infected with RSV had twice as many emergency room visits and 6 times more hospitalizations than those with seasonal influenza virus infections (23). The reasons why RSV has a tendency toward increased frequency and severity of distal small airway disease in infants compared with other etiologies are unknown.

In vitro and in vivo studies have established that ciliated cells of the human large cartilaginous airways are important targets for RSV infection. The ciliated airway epithelium serves an important role in maintaining lung health, as it provides a mechanical barrier against inhaled pathogens and contributes to clearance by facilitating MCT. Precisely how RSV infection of the airway epithelium leads to airway disease is poorly defined, but has been attributed to both direct virus-mediated epithelial cell cytopathology and exaggerated host immunopathology, especially excessive neutrophil-associated inflammation (24). Other consequences of RSV infection, such as incidence of wheezing and possible skewing of future immune responses, have been reported (25, 26). Clinical and preclinical studies have greatly increased our understanding of RSV pathogenesis, but the early initiating aspects of RSV infection of the airway epithelium and the relationship to subsequent airway pathology remain poorly defined.

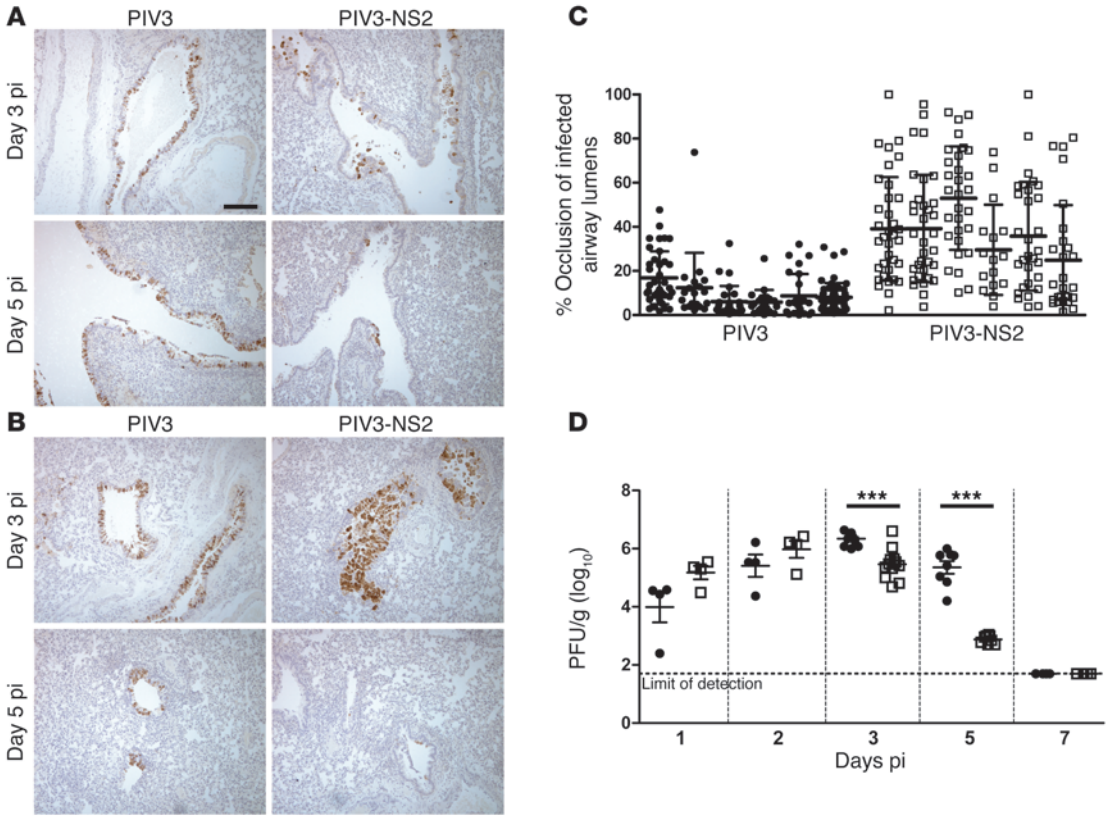

Figure 8

Distal airway obstruction and accelerated clearance of virus infection in hamsters infected by PIV3-NS2. (**A** and **B**) Representative images of histologic cross sections of hamster large airways (**A**) and small airways (**B**) 3 days and 5 days after infection with PIV3 or PIV3-NS2. Note the rapid loss of PIV3-NS2–infected cells from airways at 5 days pi, a time when PIV3 infection remained robust. Scale bar: 100 μm. (**C**) Morphometric quantitative analysis of distal airway cell accumulation in hamsters infected with PIV3 or PIV3-NS2 by measuring the percentage of cross-sectional airway lumen surface area occupied by virus antigen–positive cells at day 3 pi. Histologic, antigen-stained whole lung sections from 6 animals were measured. Each column represents an individual animal, and each symbol represents occlusion of an individual airway. Statistical analysis of the mean occlusion values of the two groups was used to determine significance. $P < 0.01$, Mann-Whitney *U* test. (**D**) Whole lung virus loads in hamsters infected with PIV3 (black circles) or PIV3-NS2 (white squares) measured over time, demonstrating a more rapid clearance of PIV3 infection when the virus expressed RSV NS2. Data (mean ± SEM) represent 3 independent experiments with a total of 4 to 9 animals per time point. All viruses expressed GFP. ***$P < 0.0001$, unpaired *t* test.

Investigating the role of the airway epithelium in RSV pathogenesis has been impeded by the scarcity of representative models of polarized and differentiated airway epithelium that are both susceptible to human RSV infection and mimic the outcomes of infection observed in RSV-infected human airways in vivo. Indeed, most experiments modeling RSV infection of the airway epithelium rely on transformed, non-polarized epithelial cell lines, which do not resemble the differentiated architecture of airway epithelium in vivo. The widely available in vivo models, particularly small rodents, also poorly reproduce the consequences of RSV infection observed in human airways, largely due to low infectivity of the conducting airway epithelium by RSV. Species-specific RSV equivalents used in appropriate permissive hosts, such as bovine RSV in calves, are useful models for understanding RSV pathogenesis, but differences between the human and animal viruses and the human and animal hosts have been documented and can complicate such analyses (27).

In the present study, we combined in vitro and in vivo models of differentiated airway epithelium to assess the impact of RSV infection on the integrity and function of the ciliated airway epithelium. Using cultures of primary pseudostratified HAE cells that closely resembled the epithelium of authentic airway tissue, we showed that RSV infection of human ciliated cells resulted in the development of a rounded cell morphology and distinct apical surface cytopathology, followed by extrusion of the infected cells from the epithelium. These effects were not observed in ciliated cells infected by PIV3 or several other respiratory paramyxoviruses. Once infected ciliated cells shed from the epithelium, these cells were incorporated into mucus secretions and underwent cell death. The shed cells and associated mucus secretions were transported across the airway surface by coordinated cilia beat.

The use of RSV gene-deletion mutants revealed that these effects were due to expression of the RSV NS2 protein. Specifically, whereas ciliated cells infected by RSV became rounded, ciliated cells infected with RSVΔNS2 maintained columnar morphology and remained embedded within the intact epithelium. Because PIV3 also targeted ciliated cells but did not cause the cell rounding phenotype, we used PIV3 as a vector to express RSV genes in ciliated cells. This novel approach to study virus gene expression in ciliated cells demonstrated that RSV NS2 expressed

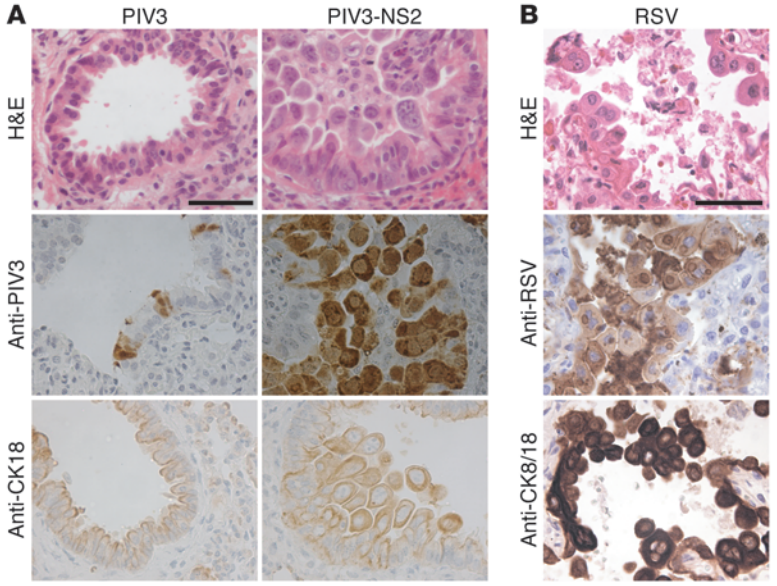

Figure 9
Shed epithelial cells infected by PIV3-NS2 into hamster lower conducting airways resembles shed epithelial cells in RSV-infected human infants. (**A**) Representative images from histologic cross sections of hamster distal airways infected with PIV3 and PIV3-NS2. Sections were stained with H&E, or with antibody against PIV3 to identify PIV3-infected cells, or with an antibody against cytokeratin 18 (CK18) to identify epithelial cells at day 3 pi. Scale bar: 50 μm. (**B**) Sample images of histologic cross sections of human lower airways obtained postmortem from a patient naturally infected by RSV. Sections were stained with H&E, or with an RSV-specific antibody to detect infected cells, or with a CK8/18 antibody to detect epithelial cells. Scale bar: 50 μm. The smaller-diameter distal airways of both hamster and human demonstrate virus antigen–positive cells that have shed and accumulated in the lumen, often sufficient to have caused airway occlusion.

by PIV3 caused morphologic changes in infected ciliated cells indistinguishable from those infected by RSV. Taken together, these findings identify expression of RSV NS2, in the context of either RSV or PIV3 infection, as sufficient to induce rounded morphology in ciliated cells.

We used PIV3-NS2 and control viruses to investigate the significance of these findings in vivo using the hamster model. In the hamster nasal cavity, PIV3 recombinant viruses infected only ciliated cells of the respiratory epithelium, and only PIV3-NS2 caused ciliated cell rounding, membrane cytopathology, and cell extrusion, similar to our findings in HAE after RSV or PIV3-NS2 infection.

Infection of the hamster lower airway epithelium with PIV3-NS2, but not PIV3, also resulted in rounding and shedding of the infected cells from the epithelium into the airway lumen. In the large airways of hamsters infected with PIV3-NS2, infected cells shed from the epithelium rarely accumulated in the airway lumen, suggesting that the majority of shed cells were rapidly and effectively cleared from the lumen, presumably by mechanical airway clearance mechanisms. In the smaller-diameter airways, shed cells accumulated in the airway lumen, suggesting that clearance of shed cells from the small airway lumens was less efficient compared with clearance from the larger airways. These effects were most pronounced in the small airways of hamsters 2 to 3 days after infection by PIV3-NS2, and accumulations of detached virus antigen–positive cells were easily detected occluding the small airway lumens, reminiscent of bronchiolar airway occlusions observed in the small airways of young infants infected by RSV. We also note that studies with RSV-infected infants have described infection of the larger airways as patches or clusters of infected cells, compared with more robust circumferential infection reported in the distal airway epithelium (10, 28). Our in vivo studies with PIV3-NS2 suggest that patchy infection in large airways may represent continuous shedding and clearance of infected cells in these regions, while shedding and accumulation may perpetuate infection in the distal airways.

The combination of small-diameter airway lumens and the swollen volume of shed cells in the distal airway regions of hamsters after PIV3-NS2 infection likely contributes to the development of airway occlusion. This finding has clear implications for RSV infection of human infants, where the very narrow distal airway lumens of the still-developing infant lung have been proposed to increase vulnerability of the distal airway regions to obstruction (29). We did note in our studies that cells shedding into the hamster lower airways were pleomorphic and unusually swollen compared with cells shedding from HAE or into the hamster nasal respiratory epithelium. The differences in morphology and size of shed cells following PIV3-NS2 infection may reflect differences in the responses of epithelial cells distributed in the lower versus upper airways. Alternatively, the swollen pleomorphic cells in lower airways may represent other epithelial cell types present in the lower but not upper airways, which, when infected by PIV3-NS2, respond differently to infection compared with ciliated cells. A potential candidate for such a cell type is the non-ciliated columnar club (Clara) cell. While club cells are rarely present in the nasal epithelium, they are present in hamster and human lower airways, with club cell density increasing as airways descend into the distal bronchiolar airway regions (30, 31). Indeed, while only ciliated cells of the nasal respiratory epithelium were infected by PIV3 and PIV3-NS2, in the lower airways, both ciliated and club cells were infected by these viruses. RSV also infects both ciliated and non-ciliated cells of the lower airways of humans (10, 12), and both cell types are infected in the small airways of calves and lambs experimentally infected with RSV (32, 33). Thus, the differences in morphology between cells shed into the lower versus upper airways might be due to PIV3-NS2 infection of club cells. Regardless of the specific epithelial cell types infected by PIV3-NS2 in the different airway regions, we suggest that the combination of smaller diameter of airway lumens in the bronchioles and the expanded volume of cells shed into these airway regions enhances the likelihood that shed cells would accumulate in and occlude distal airways.

Unusual epithelial cell morphology has been described for RSV-infected humans and bovine RSV–infected calves (11, 12, 32), and sloughing of virus antigen–positive cells caused small airway occlusion in ovine and baboon models of RSV infection (33–35). The loss of cilia and disorganization of cilia basal bodies noted in human ciliated cells infected by RSV and PIV3-NS2 was also reported in a bovine model of RSV infection (32). Ciliary dyskinesia and apical membrane damage have been reported in RSV-infected human ciliated airway epithelium cultures (36). Thus, in

several appropriate animal models of RSV infection as well as retrospective analysis of human cases of RSV infection, shedding of pleomorphic, virus antigen–positive epithelial cells, especially in the smaller-diameter distal airways, appears to be a characteristic hallmark of RSV infection. We propose that RSV NS2 may be a major contributor to the development of these early pathologic findings following RSV infection.

Accumulation of shed cells in the distal lower airways of hamsters infected with PIV3-NS2 suggests that RSV NS2–induced cell shedding might have importance for the initiation of RSV-associated disease. RSV bronchiolitis is closely associated with small airway obstruction, resulting in air trapping distal to the obstruction and increased airway resistance (37, 38). Classically, the obstructive material has been considered to be a mixture of necrotic epithelial cells, mucus secretions, and inflammatory cell exudate. However, autopsy specimens from RSV-infected patients, including those described in this study, rarely show the presence of mucus plugs in the small airways but consistently show unusual pleomorphic epithelial cells positive for virus antigen in the airway lumen. These human autopsy specimens from patients infected with RSV combined with hamsters infected by PIV3-NS2 emphasize the potential significance of shed and accumulated epithelial cells as major contributors to small airway obstruction following RSV infection.

The present study suggests that RSV has an unusual and perhaps unique ability to induce epithelial cell shedding, and that NS2-induced cell shedding may be an important factor in RSV pathogenesis. However, the dramatic distal airway plugging in PIV3-NS2–infected hamsters was transient, as maximal occlusion occurred at day 3 pi but was cleared by day 5 pi. Obstruction of small airways was also not associated with increased clinical disease in hamsters. The lack of disease associated with PIV3 (and RSV) infection in rodent models likely reflects their semi-permissive nature for virus replication, with relatively low whole lung viral titers and relatively short durations of infection. In contrast, RSV infection of humans results in substantially higher virus titers, and virus shedding can continue for up to several weeks (39, 40). Primary RSV infection in humans is nearly always symptomatic, and in this more permissive setting, it is reasonable to expect that RSV NS2–promoted obstruction of small airways with shed epithelial cells would be longer lived, promoting enhanced infection and inflammation and contributing to increased disease severity. Interestingly, we also noted that PIV3-NS2 infection was cleared from hamster lungs more rapidly than was PIV3. This was evident by histologic analysis, which showed that despite the extensive infection and airway occlusions associated with PIV3-NS2 on day 3 pi, the infected cells were largely cleared by day 5 pi. In contrast, in animals infected with PIV3, there were abundant infected cells on both days 3 and 5 pi. Consistent with this, quantification of whole lung viral titers confirmed that PIV3-NS2 was cleared more rapidly than PIV3, even though both viruses reached similar peak titers by days 2–3 pi.

Previous studies have demonstrated that the RSV NS proteins enhance viral replication. Recombinant RSV deleted for 1 or both NS genes resulted in viruses with severely attenuated growth in vitro and in vivo (41–43). Deletion of either the NS1 or NS2 gene attenuated human RSV in chimpanzees (42, 44). The NS proteins have also been shown to interfere with a number of antiviral host responses aimed at reducing the extent of virus replication, most notably types I and III IFN pathways. The mechanisms by which NS1 and NS2 inhibit IFN responses are complex, involving both coordinated and independent functions of the NS proteins (41, 45–48). Both proteins have also been implicated in inhibiting apoptosis (49), and RSV NS2 was reported to enhance induction of NF-κB (19). Although some effects of the NS proteins appear to involve synergy between NS1 and NS2, this did not appear to be the case in the present study. Here, the morphologic and shedding phenotype attributed to RSV NS2 appeared to be independent of, and unaffected by, NS1. While the precise mechanism of NS2-induced morphologic consequences remains unknown, we speculate that these events are not directly related to the ability of NS2 to modify IFN responses.

The mechanism by which RSV NS2 exerts its effects on epithelial cell rounding and shedding remains to be explored. Based on changes in columnar cell morphology, it would be reasonable to speculate that RSV NS2 may exert effects on cytoskeletal structures. Indeed, RSV has been reported to have effects on intermediate filaments and actin filament structures (50–53). The influence of RSV NS2 on cytoskeletal elements represents a potential mechanism for cell rounding following RSV infection and will be the focus of future studies. Comparison of PIV3-NS2 infection of epithelial cell line monolayers with PIV3 or PIV3-NS1 have thus far failed to reveal a morphologic phenotype attributable to RSV NS2 (data not shown), suggesting that the differentiated state of the columnar airway epithelial cells may be a critical component of NS2-induced cell rounding. The use of differentiated airway models such as HAE will therefore be important for understanding how RSV NS2 modifies airway epithelial cells, resulting in the shedding of infected cells into the airway lumen.

In summary, we present evidence that infection of ciliated cells in HAE by RSV results in cell rounding, disruption of the cilia apparatus, active shedding of individual infected cells, and delay of cell death until infected cells are shed from the epithelium. By performing loss-of-function and gain-of-function experiments, we attribute these consequences of infection to the RSV NS2 protein. Using PIV3 as a vector for RSV NS2, we confirmed these findings in an in vivo hamster model of infection. Expression of RSV NS2 in vivo resulted in accelerated clearance of infection, and we propose that NS2-induced cell shedding acts as a novel clearance mechanism to remove infected cells from both the airway epithelium and the lumen. In the smaller-diameter distal airways, however, NS2-induced shedding contributed to acute airway obstruction, which was strikingly reminiscent of the airway plugging that occurs during RSV bronchiolitis in infants. Although other respiratory viruses also cause bronchiolitis in young children, we suggest that NS2-mediated cell shedding and subsequent airway obstruction may contribute to the increased incidence and severity of RSV-associated bronchiolitis compared with other viral etiologies. The notion that RSV NS2 may be a pathogenesis factor increasing the likelihood of small airway obstruction as a precursor to bronchiolitis identifies NS2 as a potential therapeutic target for limiting the severity and frequency of RSV bronchiolitis, particularly in infants. It also suggests that deletion of the NS2 gene may be desirable in live-attenuated RSV vaccine candidates (54). Future studies are needed to explore whether RSV NS2–mediated shedding of infected cells affects the development of immunity to RSV infection, and whether manipulation of NS2-promoted epithelial cell shedding may serve as a therapeutic target for reducing the severity of distal airway disease in RSV-infected infants.

Methods

Cells

HAE cells were isolated by the University of North Carolina Cystic Fibrosis Center Cell Culture and Tissue Procurement Core from tracheobronchial airway specimens obtained from patients, provided by the National Disease Research Interchange or as excess tissue following lung transplantation. All protocols were approved by the University of North Carolina at Chapel Hill Institutional Review Board. Primary epithelial cells derived from single patient sources were plated on permeable Transwell-Col supports (12-mm diameter; Corning Inc.) and grown in custom media at an air-liquid interface for 8 to 10 weeks to form differentiated, polarized cultures as previously described (55). HEp2 cells (ATCC) were maintain in MEM (Gibco) supplemented with 10% fetal bovine serum (Foundation; Gemini Bio-Products). LLC-MK2 cells (ATCC) were maintained in DMEM (Gibco) supplemented with 10% fetal bovine serum (Foundation; Gemini Bio-Products).

Animals

In vivo animal studies used Golden Syrian hamsters (Harlan), and all procedures were conducted in accordance with the NIH Guide for the Care and Use of Laboratory Animals and using animal study protocols approved by the Animal Care and Use Committee of the National Institute of Allergy and Infectious Diseases and the Institutional Animal Care and Use Committee of the University of North Carolina at Chapel Hill.

Viruses

All viruses used in this study were derived from cDNA (recombinant) and contain a GFP insertion as an additional gene, unless otherwise mentioned.

Recombinant HMPV (strain CAN97-83), PIV5 (strain W3A; provided by Robert Lamb, Northwestern University, Evanston, Illinois, USA), and SeV (provided by Daniel Kolakofsky, University of Geneva School of Medicine, Geneva, Switzerland) were described previously (56–58). RSV Memphis 37 strain was isolated from a pediatric case of bronchiolitis and has been described previously (39). This virus is a primary low-passage clinical isolate, not a recombinant virus, and does not express GFP.

Wild-type RSV, RSVΔNS1, RSVΔNS2, and RSVΔNS1/2 are derivatives of the A2 strain and were constructed and described previously (44, 59–61). Each of these RSV constructs express the GFP gene as an additional gene inserted between the RSV P and M genes. Wild-type RSV and all mutants were amplified in HEp2 cells stably expressing the V gene from SV5 (62). The SV5-V plasmid was provided by Richard Randall (University of St. Andrews, St. Andrews, United Kingdom).

PIV3 is a derivative of the JS strain engineered to express the GFP gene as an additional gene inserted between the PIV3 P and M genes, as has been described previously (63, 64). Codon-optimized RSV NS1 or NS2 genes were synthesized (DNA2.0) and inserted into the PIV3 viral genome between the hemagglutinin-neuraminidase (HN) and viral polymerase (L) genes using cloning methods similar to those previously used to express CFTR and rhAFP in this genome region (65, 66). A unique EagI restriction site was generated in the non-coding region downstream of the HN gene in the PIV3 subgenomic cDNA. The NS1 or NS2 coding sequence was amplified using RT-PCR from plasmids expressing codon-optimized NS1 or NS2, cloned into a pCR-Blunt II-TOPO vector (Invitrogen) and sequenced. The following primer sets were used: NS1 sense (5′-CCGCGGCCACCATGGGCAGCAATAGTCTC-3′), NS1 antisense (5′-GGGCCCGAGTTATGGGTTCAGGTCAA-3′), NS2 sense (5′-CCGCGGCCACAATGGATACCACGC-3′), and NS2 antisense (5′-GGGCCCCTCGAGTCAAGGGTTCAA-3′) (the underlined portions represent SacII and ApaI restriction sites). Using the SacII and ApaI restriction sites, NS1 or NS2 was inserted into a vector following a linker sequence consisting of the PIV3 gene-end, intergenic, and gene-start transcription regions, flanked at both ends by EagI sites. This cassette was then inserted using the EagI sites into the full-length PIV3GFP antigenomic cDNA, and the resulting genomes were designated PIV3-NS1 or PIV3-NS2. A PIV3 genome expressing both NS1 and NS2 was also generated by inserting the RSV NS1 and NS2 genes together into PIV3 between the HN and L genes using similar methods. From the linker vector containing NS1, a sequence consisting of the EagI restriction site, PIV3 linker region, and NS1 gene was PCR amplified using the NS1 sense primer (5′-CGAATTGGCGGCCGAAAATA-3′) and the NS1 antisense primer (5′-CAGGAGTTCAGCACGATGGGGGCCCGAGTTATGGGT-3′), destroying the 3′ EagI site and creating an 18-bp overhang. From the linker vector containing NS2, a sequence consisting of the PIV3 linker region, the NS2 gene, and the EagI restriction site was amplified using the NS2 sense primer (5′-GCTGAACTCCTGCATCGTAAAATAAGAAAAACTTAG-3′) and the NS2 antisense primer (5′-ACTTGGCCCAAGCTTGAGTA-3′), destroying the 5′ EagI site and adding the complementary 18-bp overhang. These 2 fragments were combined in a fusion reaction using the NS1 sense and NS2 antisense primers, and the resulting fragment was cloned into a pCRBluntII TOPO vector (Invitrogen) and sequenced. The final fragment consisted of a PIV3 linker region, the RSV NS1 gene, a second PIV3 linker region, and the RSV NS2 gene, flanked by EagI sites. This cassette was then inserted using the EagI sites into the full-length PIV3GFP antigenomic cDNA, creating PIV3-NS1/2. Each insert was designed to retain the "rule of 6," in which a genome length with a multiple of 6 nucleotides is required for PIV3 genome replication. All viruses were rescued and amplified in LLC-MK2 cells using methods described previously (63) and sequenced.

Viral inoculations and growth

In vitro studies. The apical surfaces of HAE were rinsed with PBS to remove excess airway secretions. Virus inoculum diluted in serum-free DMEM (Gibco; 100 μl per 12 mm well) was applied to the apical surface of HAE for 2 hours at 37°C, then removed by aspiration. The apical surfaces were rinsed with PBS, and the cultures were incubated at 37°C. Viral growth kinetics were determined by performing apical surface washes with 300 μl of serum-free DMEM, which were harvested after 30 minutes at 37°C and stored at –80°C until analysis. RSV viral titers in the apical washes were determined on HEp2 cells by titration and counting GFP-positive cells 24 hours pi. PIV3 viral titers were determined using a 50% tissue culture infectious dose ($TCID_{50}$) assay on LLC-MK2 cell monolayers, with positive wells scored by GFP expression. En face fluorescent images of GFP-positive cells in HAE were captured using a Leica DMIRB Inverted Fluorescent Microscope equipped with a Retiga 1300 CCD camera (Q-Imaging). The proportion of the surface area of epithelium positive for GFP was determined by pixelating a black-and-white image, calculating the percentage of black pixels using ImageJ software (NIH) for 5 fields per culture, and averaging the results.

In vivo studies. Ten- to twelve-week-old female Golden Syrian hamsters (Harlan) were transiently anesthetized (methoxyflurane) and inoculated intranasally with 10^6 PFU of PIV3, PIV3-NS1, or PIV3-NS2 in 100 μl serum-free L-15 Leibovitz medium (Gibco). Animals were euthanized and respiratory tissues harvested at the pi times indicated in the figures, for analysis of virus titers or histologic assessment. For virus titrations, whole lungs or nasal turbinates were weighed and homogenized in PBS. Viral titers were determined by standard plaque assay of the clarified supernatants, as previously described (67).

Histology and immunoprotocols

HAE cultures fixed in 4% paraformaldehyde in PBS were paraffin embedded, and 5-μm-thick histological sections were prepared. Sections were stained with H&E or Richardson's stain. Immunodetection

of RSV antigen and β-tubulin IV was performed by blocking sections in 3% BSA in PBS, followed by incubation with primary antibodies against GFP (rabbit polyclonal; Abcam) and β-tubulin IV (mouse monoclonal; Sigma-Aldrich). Immunoreactivity was detected using an anti-rabbit IgG conjugated to Alexa Fluor 488 and an anti-mouse IgG conjugated to Alexa Fluor 594 (Molecular Probes). To preserve and visualize apical secretions of HAE, cultures were fixed in the alcohol-based fixative Omnifix (FR Chemical) as previously described (68) and stained with H&E. Immunohistochemistry for viral antigens were performed by blocking sections in 3% BSA and incubating with primary antibodies against RSV (anti-RSV goat polyclonal; Meridian Life Sciences) or PIV3 (anti-PIV3 rabbit serum raised against sucrose-gradient-purified PIV3; ref. 69). Immunoreactivity was detected using anti-goat or anti-rabbit secondary antibodies conjugated to HRP, visualized using 3,3′-diaminobenzidine (Sigma-Aldrich), and counterstained with hematoxylin. For TEM studies, HAE cultures were fixed in glutaraldehyde solution, then in an osmium tetroxide solution to preserve the hydrated external environment of the HAE, as previously described (68), and visualized using standard TEM techniques.

For histologic examination of hamster tissues, excised nasal turbinates or whole lungs were immersion-fixed in 10% neutral-buffered formalin and embedded in paraffin, and histological sections were generated for examination and staining. Sections were stained with H&E. Immunodetection of viral antigen was performed using the anti-PIV3 rabbit serum mentioned above. To identify epithelial cells, a cytokeratin 18 antibody was used (mouse monoclonal; Abcam). Primary antibodies were detected using anti-mouse or anti-rabbit antibodies conjugated to HRP (Jackson ImmunoResearch Laboratories), visualized using 3,3′-diaminobenzidine (Sigma-Aldrich), and counterstained with hematoxylin.

RSV infection in human airways was determined in lung tissue obtained from infants with complete DiGeorge Syndrome naturally infected by RSV, and tissue was provided by the Duke University Pathology Specimen Repository in accordance with Duke University IRB protocols. RSV and cytokeratin 8/18 immunoreactivity was performed on histological sections using a Leica Bond-III automated stainers (Leica Microsystems Inc.). Following antigen retrieval with Novocastra Bond Epitope Retrieval 1 solution (Leica Microsystems), sections were incubated with a primary antibody against RSV antigen (clones 5H5N, 2G12, 5A6, IC3; Vector Laboratories) and detected with the Novocastra Bond Polymer Refine Detection system (Leica Microsystems). Immunostaining for cytokeratin 8/18 used a proteinase K epitope retrieval solution (Dako North America Inc.), the primary antibody Novocastra cytokeratin 8/18 monoclonal antibody (clone 5D3; Leica Microsystems), and detection with the Novocastra Bond Polymer Refine Detection system.

Morphometric analysis of cell height and airway occlusion

XZ confocal images were acquired using a Leica SP5 confocal microscope. XZ images through the tallest region of a GFP-positive infected cell in fixed but unprocessed HAE cultures were imported into ImageJ software (NIH), where pixel height was measured and converted to microns using the electronic magnification measurement bar from the confocal image. A minimum of 100 infected cells were measured from at least 3 individual donors.

The height of infected cells in the nasal respiratory tissue was determined by measuring pixel height of infected cells in images from fixed, viral antigen–stained sections using ImageJ software (NIH) and converting to microns.

Occlusion of airways was determined by imaging infected airway regions from fixed, viral antigen–stained sections, converting to black-and-white images, pixelating, and calculating the percentage of black pixels within the airway lumen using ImageJ software. Airway occlusions were measured from 6 individual animals harvested on day 3 pi. All airways with antigen-positive cells (mean: ~30 airways per animal), except those larger than 1 mm in diameter (~1 airway per animal), were measured, regardless of number of infected cells or extent of infection per airway.

Cell shedding

Cell shedding was quantified by determining the amount of dsDNA in apical washes of HAE using the Quant-It PicoGreen dsDNA kit (Invitrogen). Apical washes were performed with 300 μl serum-free DMEM for 30 minutes at 37°C. Washes were harvested and stored at –80°C prior to analysis. Samples were diluted 5-fold in Tris-EDTA buffer, and dsDNA was measured in duplicate following the manufacturer's instructions using a 96-well plate format. dsDNA concentration per sample was calculated based on fluorescence of a titrated dsDNA standard.

Percentage of area ciliated

Following removal of apical washes for titer and cell shedding assays, HAE cultures were allowed to come to room temperature for 15 minutes to normalize cilia beat frequency, and 100 μl PBS was added apically. HAE cultures were placed on an inverted phase contrast microscope (TE2000; Nikon) using a ×20 objective, and high-speed (125-Hz) video images were captured with an 8-bit black-and-white camera (GS-310 Turbo; Megaplus). The analog signal was digitized via an analog-to-digital converter board (A/D; National Instruments). A digital computerized analysis system was used to analyze the acquired video images, using software based on Sisson-Ammons Video Analysis (70).

MCT rates

Following removal of apical washes for titer and shedding assays, green fluorescent microspheres (0.02% vol/vol, 1 μm; Invitrogen) were added to the apical surface and HAE cultures were incubated at 37°C. Time-lapse fluorescent images were obtained for 3 s using a Leica DMIRB Inverted Fluorescent Microscope equipped with a Retiga 1300 charge-coupled device camera (Q-Imaging). The rate of microsphere displacement was calculated as previously described (65).

Statistics

Statistical analysis of the data was performed using 2-tailed unpaired *t* test, ANOVA, or Mann-Whitney *U* test, as indicated in the figure legends. $P < 0.05$ was considered statistically significant unless otherwise noted.

Study approval

Protocols for the use of animals in these studies were reviewed and approved by the University of North Carolina at Chapel Hill IACUC (approval ID 11-118.0) and the Animal Care and Use Committee of the National Institute of Allergy and Infectious Diseases (NIAID ASP LID34E). Protocols for human cell culture were reviewed by the University of North Carolina at Chapel Hill Office of Human Research Ethics, which determined that the use of cells did not constitute human subject research as defined under federal regulations (45 CFR 46.102 [d or f] and 21 CFR 56.102[c][e][l]) and did not require institutional review board approval. Protocols for using existing human autopsy specimens were reviewed by the Duke University Institutional Review Board, which determined that the protocols met the definition of research not involving human subjects as described in 45 CFR 46.102(f), 21 CFR 56.102(e), and 21 CFR 812.3(p) and satisfied the Privacy Rule as described in 45CFR164.514.

Acknowledgments

The authors thank the Directors and teams of the UNC Cystic Fibrosis Center Core Facilities used during these studies: the Tissue Procurement and Cell Culture Core, the Morphology

and Morphometry Core, and the Michael Hooker Microscopy Facility. We thank Kui Shen of the Computational Biology Section of the NIAID, NIH, for assistance with statistical analysis. We also thank Shirin Munir for the RSV NS1 and NS2 cDNAs, Richard Randall for providing the SV5-V plasmid, Robert Lamb for providing the PIV5-GFP virus, and Daniel Kolakofsky for providing the SeV-GFP virus. These studies were funded by grants from the UNC University Research Council and the NIH (R01HL103940, R01HL77844, P50HL084934, T32AI007419). U.J. Buchholz, C.L. Luongo, L. Yang, and P.L. Collins were supported by the Intramural Research Program of the NIAID, NIH. R.M. Liesman is a Howard Hughes Medical Institute (HHMI) Med-into-Grad Scholar supported in part by a grant to the University of North Carolina at Chapel Hill from HHMI through the Med-into-Grad Initiative.

Received for publication August 30, 2013, and accepted in revised form February 13, 2014.

Address correspondence to: Raymond J. Pickles, Cystic Fibrosis and Pulmonary Research and Treatment Center, University of North Carolina at Chapel Hill, 7021 Thurston Bowles Building, Chapel Hill, North Carolina 27599-7248, USA. Phone: 919.966.7044; Fax: 919.966.5178; E-mail: branston@med.unc.edu.

1. Glezen WP, Taber LH, Frank AL, Kasel JA. Risk of primary infection and reinfection with respiratory syncytial virus. *Am J Dis Child*. 1986;140(6):543–546.
2. Hall CB, et al. The burden of respiratory syncytial virus infection in young children. *N Engl J Med*. 2009; 360(6):588–598.
3. Nair H, et al. Global burden of acute lower respiratory infections due to respiratory syncytial virus in young children: a systematic review and meta-analysis. *Lancet*. 2010;375(9725):1545–1555.
4. Krilov LR. Safety issues related to the administration of ribavirin. *Pediatr Infect Dis J*. 2002;21(5):479–481.
5. Davison C, Ventre KM, Luchetti M, Randolph AG. Efficacy of interventions for bronchiolitis in critically ill infants: a systematic review and meta-analysis. *Pediatr Crit Care Med*. 2004;5(5):482–489.
6. Garrison MM, Christakis DA, Harvey E, Cummings P, Davis RL. Systemic corticosteroids in infant bronchiolitis: a meta-analysis. *Pediatrics*. 2000; 105(4):E44.
7. van Woensel JB, Vyas H, STAR Trial Group. Dexamethasone in children mechanically ventilated for lower respiratory tract infection caused by respiratory syncytial virus: a randomized controlled trial. *Crit Care Med*. 2011;39(7):1779–1783.
8. Committee on Infectious Diseases. From the American Academy of Pediatrics: Policy statements — modified recommendations for use of palivizumab for prevention of respiratory syncytial virus infections. *Pediatrics*. 2009;124(6):1694–1701.
9. Null D Jr, et al. Safety and immunogenicity of palivizumab (Synagis) administered for two seasons. *Pediatr Infect Dis J*. 2005;24(11):1021–1023.
10. Johnson JE, Gonzales RA, Olson SJ, Wright PF, Graham BS. The histopathology of fatal untreated human respiratory syncytial virus infection. *Mod Pathol*. 2007;20(1):108–119.
11. Shedden WI, Emery JL. Immunofluorescent evidence of respiratory syncytial virus infection in cases of giant cell bronchiolitis in children. *J Pathol Bacteriol*. 1965;89:343–347.
12. Welliver TP, Reed JL, Welliver RC Sr. Respiratory syncytial virus and influenza virus infections: observations from tissues of fatal infant cases. *Pediatr Infect Dis J*. 2008;27(10 suppl):S92–S96.
13. Villenave R, et al. In vitro modeling of respiratory syncytial virus infection of pediatric bronchial epithelium, the primary target of infection in vivo. *Proc Natl Acad Sci U S A*. 2012;109(13):5040–5045.
14. Zhang L, Peeples ME, Boucher RC, Collins PL, Pickles RJ. Respiratory syncytial virus infection of human airway epithelial cells is polarized, specific to ciliated cells, and without obvious cytopathology. *J Virol*. 2002;76(11):5654–5666.
15. Sims AC, Baric RS, Yount B, Burkett SE, Collins PL, Pickles RJ. Severe acute respiratory syndrome coronavirus infection of human ciliated airway epithelia: role of ciliated cells in viral spread in the conducting airways of the lungs. *J Virol*. 2005; 79(24):15511–15524.
16. Thompson CI, Barclay WS, Zambon MC, Pickles RJ. Infection of human airway epithelium by human and avian strains of influenza a virus. *J Virol*. 2006;80(16):8060–8068.
17. Zhang L, Collins PL, Lamb RA, Pickles RJ. Comparison of differing cytopathic effects in human airway epithelium of parainfluenza virus 5 (W3A), parainfluenza virus type 3, and respiratory syncytial virus. *Virology*. 2011;421(1):67–77.
18. Scull MA, et al. Avian Influenza virus glycoproteins restrict virus replication and spread through human airway epithelium at temperatures of the proximal airways. *PLoS Pathog*. 2009;5(5):e1000424.
19. Spann KM, Tran KC, Collins PL. Effects of nonstructural proteins NS1 and NS2 of human respiratory syncytial virus on interferon regulatory factor 3, NF-κB, and proinflammatory cytokines. *J Virol*. 2005;79(9):5353–5362.
20. Liu C, Sharp E, Collins J. Studies on the pathogenesis of parainfluenza type 3 virus infection in hamsters. *Arch Gesamte Virusforsch*. 1968;24(3):203–219.
21. García CG, et al. Risk factors in children hospitalized with RSV bronchiolitis versus non-RSV bronchiolitis. *Pediatrics*. 2010;126(6):e1453–e1460.
22. Hervas D, Reina J, Yanez A, del Valle JM, Figuerola J, Hervas JA. Epidemiology of hospitalization for acute bronchiolitis in children: differences between RSV and non-RSV bronchiolitis. *Eur J Clin Microbiol Infect Dis*. 2012;31(8):1975–1981.
23. Bourgeois FT, Valim C, McAdam AJ, Mandl KD. Relative impact of influenza and respiratory syncytial virus in young children. *Pediatrics*. 2009; 124(6):e1072–e1080.
24. McNamara PS, Ritson P, Selby A, Hart CA, Smyth RL. Bronchoalveolar lavage cellularity in infants with severe respiratory syncytial virus bronchiolitis. *Arch Dis Child*. 2003;88(10):922–926.
25. Blanken MO, et al. Respiratory syncytial virus and recurrent wheeze in healthy preterm infants. *N Engl J Med*. 2013;368(19):1791–1799.
26. Sigurs N, et al. Asthma and allergy patterns over 18 years after severe RSV bronchiolitis in the first year of life. *Thorax*. 2010;65(12):1045–1052.
27. Bossert B, Conzelmann KK. Respiratory syncytial virus (RSV) nonstructural (NS) proteins as host range determinants: a chimeric bovine RSV with NS genes from human RSV is attenuated in interferon-competent bovine cells. *J Virol*. 2002; 76(9):4287–4293.
28. Welliver TP, et al. Severe human lower respiratory tract illness caused by respiratory syncytial virus and influenza virus is characterized by the absence of pulmonary cytotoxic lymphocyte responses. *J Infect Dis*. 2007;195(8):1126–1136.
29. Hislop AA, Haworth SG. Airway size and structure in the normal fetal and infant lung and the effect of premature delivery and artificial ventilation. *Am Rev Respir Dis*. 1989;140(6):1717–1726.
30. Boers JE, Ambergen AW, Thunnissen FB. Number and proliferation of clara cells in normal human airway epithelium. *Am J Respir Crit Care Med*. 1999; 159(5 pt 1):1585–1591.
31. Christensen TG, Breuer R, Hornstra LJ, Lucey EC, Snider GL. The ultrastructure of hamster bronchial epithelium. *Exp Lung Res*. 1987;13(3):253–277.
32. Bryson DG, Platten MF, McConnell S, McNulty MS. Ultrastructural features of lesions in bronchiolar epithelium in induced respiratory syncytial virus pneumonia of calves. *Vet Pathol*. 1991; 28(4):293–299.
33. Derscheid RJ, Ackermann MR. Perinatal lamb model of respiratory syncytial virus (RSV) infection. *Viruses*. 2012;4(10):2359–2378.
34. Olivier A, Gallup J, de Macedo MM, Varga SM, Ackermann M. Human respiratory syncytial virus A2 strain replicates and induces innate immune responses by respiratory epithelia of neonatal lambs. *Int J Exp Pathol*. 2009;90(4):431–438.
35. Papin JF, et al. Infant baboons infected with respiratory syncytial virus develop clinical and pathological changes that parallel those of human infants. *Am J Physiol Lung Cell Mol Physiol*. 2013; 304(8):L530–L539.
36. Smith CM, et al. Ciliary dyskinesia is an early feature of respiratory syncytial virus infection. *Eur Respir J*. 2014;43(2):485–496.
37. Aherne W, Bird T, Court SD, Gardner PS, McQuillin J. Pathological changes in virus infections of the lower respiratory tract in children. *J Clin Pathol*. 1970;23(1):7–18.
38. Simpson W, Hacking PM, Court SD, Gardner PS. The radiological findings in respiratory syncytial virus infection in children. II. The correlation of radiological categories with clinical and virological findings. *Pediatr Radiol*. 1974;2(3):155–160.
39. DeVincenzo JP, et al. Viral load drives disease in humans experimentally infected with respiratory syncytial virus. *Am J Respir Crit Care Med*. 2010; 182(10):1305–1314.
40. Hall CB, Douglas RG Jr, Geiman JM. Respiratory syncytial virus infections in infants: quantitation and duration of shedding. *J Pediatr*. 1976;89(1):11–15.
41. Spann KM, Tran KC, Chi B, Rabin RL, Collins PL. Suppression of the induction of alpha, beta, and lambda interferons by the NS1 and NS2 proteins of human respiratory syncytial virus in human epithelial cells and macrophages [corrected]. *J Virol*. 2004; 78(8):4363–4369.
42. Whitehead SS, et al. Recombinant respiratory syncytial virus bearing a deletion of either the NS2 or SH gene is attenuated in chimpanzees. *J Virol*. 1999; 73(4):3438–3442.
43. Wright PF, et al. The interferon antagonist NS2 protein of respiratory syncytial virus is an important virulence determinant for humans. *J Infect Dis*. 2006;193(4):573–581.
44. Teng MN, et al. Recombinant respiratory syncytial virus that does not express the NS1 or M2-2 protein is highly attenuated and immunogenic in chimpanzees. *J Virol*. 2000;74(19):9317–9321.
45. Hastie ML, et al. The human respiratory syncytial virus nonstructural protein 1 regulates type I and type II interferon pathways. *Mol Cell Proteomics*.

2012;11(5):108–127.
46. Ling Z, Tran KC, Teng MN. Human respiratory syncytial virus nonstructural protein NS2 antagonizes the activation of beta interferon transcription by interacting with RIG-I. *J Virol*. 2009;83(8):3734–3742.
47. Ramaswamy M, Shi L, Varga SM, Barik S, Behlke MA, Look DC. Respiratory syncytial virus nonstructural protein 2 specifically inhibits type I interferon signal transduction. *Virology*. 2006; 344(2):328–339.
48. Swedan S, Musiyenko A, Barik S. Respiratory syncytial virus nonstructural proteins decrease levels of multiple members of the cellular interferon pathways. *J Virol*. 2009;83(19):9682–9693.
49. Bitko V, et al. Nonstructural proteins of respiratory syncytial virus suppress premature apoptosis by an NF-κB-dependent, interferon-independent mechanism and facilitate virus growth. *J Virol*. 2007; 81(4):1786–1795.
50. Bitko V, Oldenburg A, Garmon NE, Barik S. Profilin is required for viral morphogenesis, syncytium formation, and cell-specific stress fiber induction by respiratory syncytial virus. *BMC Microbiol*. 2003;3:9.
51. Burke E, Dupuy L, Wall C, Barik S. Role of cellular actin in the gene expression and morphogenesis of human respiratory syncytial virus. *Virology*. 1998; 252(1):137–148.
52. Garcia-Barreno B, Jorcano JL, Aukenbauer T, Lopez-Galindez C, Melero JA. Participation of cytoskeletal intermediate filaments in the infectious cycle of human respiratory syncytial virus (RSV). *Virus Res*. 1988;9(4):307–321.
53. Kallewaard NL, Bowen AL, Crowe JE Jr. Cooperativity of actin and microtubule elements during replication of respiratory syncytial virus. *Virology*. 2005; 331(1):73–81.
54. Luongo C, Winter CC, Collins PL, Buchholz UJ. Respiratory syncytial virus modified by deletions of the NS2 gene and amino acid S1313 of the L polymerase protein is a temperature-sensitive, live-attenuated vaccine candidate that is phenotypically stable at physiological temperature. *J Virol*. 2013; 87(4):1985–1996.
55. Fulcher ML, Gabriel S, Burns KA, Yankaskas JR, Randell SH. Well-differentiated human airway epithelial cell cultures. *Methods Mol Med*. 2005; 107:183–206.
56. Biacchesi S, Skiadopoulos MH, Tran KC, Murphy BR, Collins PL, Buchholz UJ. Recovery of human metapneumovirus from cDNA: optimization of growth in vitro and expression of additional genes. *Virology*. 2004;321(2):247–259.
57. He B, Paterson RG, Ward CD, Lamb RA. Recovery of infectious SV5 from cloned DNA and expression of a foreign gene. *Virology*. 1997;237(2):249–260.
58. Iseni F, Garcin D, Nishio M, Kedersha N, Anderson P, Kolakofsky D. Sendai virus trailer RNA binds TIAR, a cellular protein involved in virus-induced apoptosis. *EMBO J*. 2002;21(19):5141–5150.
59. Collins PL, Hill MG, Camargo E, Grosfeld H, Chanock RM, Murphy BR. Production of infectious human respiratory syncytial virus from cloned cDNA confirms an essential role for the transcription elongation factor from the 5′ proximal open reading frame of the M2 mRNA in gene expression and provides a capability for vaccine development. *Proc Natl Acad Sci U S A*. 1995;92(25):11563–11567.
60. Spann KM, Collins PL, Teng MN. Genetic recombination during coinfection of two mutants of human respiratory syncytial virus. *J Virol*. 2003; 77(20):11201–11211.
61. Teng MN, Collins PL. Altered growth characteristics of recombinant respiratory syncytial viruses which do not produce NS2 protein. *J Virol*. 1999;73(1):466–473.
62. Young DF, et al. Virus replication in engineered human cells that do not respond to interferons. *J Virol*. 2003;77(3):2174–2181.
63. Durbin AP, Hall SL, Siew JW, Whitehead SS, Collins PL, Murphy BR. Recovery of infectious human parainfluenza virus type 3 from cDNA. *Virology*. 1997;235(2):323–332.
64. Zhang L, et al. Infection of ciliated cells by human parainfluenza virus type 3 in an in vitro model of human airway epithelium. *J Virol*. 2005; 79(2):1113–1124.
65. Zhang L, et al. CFTR delivery to 25% of surface epithelial cells restores normal rates of mucus transport to human cystic fibrosis airway epithelium. *PLoS Biol*. 2009;7(7):e1000155.
66. Zhang L, et al. α-Fetoprotein gene delivery to the nasal epithelium of nonhuman primates by human parainfluenza viral vectors. *Hum Gene Ther*. 2010; 21(12):1657–1664.
67. Newman JT, et al. Sequence analysis of the Washington/1964 strain of human parainfluenza virus type 1 (HPIV1) and recovery and characterization of wild-type recombinant HPIV1 produced by reverse genetics. *Virus Genes*. 2002;24(1):77–92.
68. Kesimer M, Ehre C, Burns KA, Davis CW, Sheehan JK, Pickles RJ. Molecular organization of the mucins and glycocalyx underlying mucus transport over mucosal surfaces of the airways. *Mucosal Immunol*. 2013;6(2):379–392.
69. Bukreyev A, et al. Chimeric human parainfluenza virus bearing the Ebola virus glycoprotein as the sole surface protein is immunogenic and highly protective against Ebola virus challenge. *Virology*. 2009;383(2):348–361.
70. Sisson JH, Stoner JA, Ammons BA, Wyatt TA. All-digital image capture and whole-field analysis of ciliary beat frequency. *J Microsc*. 2003;211(pt 2):103–111.